Geophys. J. Int. (2007) **168,** 211–223 doi: 10.1111/j.1365-246X.2006.03149.x

Scattering attenuation, dispersion and reflection of *SH* waves in two-dimensional elastic media with densely distributed cracks

Yoshio Murai

Institute of Seismology and Volcanology, Faculty of Science, Hokkaido University, N-10 W-8*, Kita-ku, Sapporo* 060-0810*, Japan.*
E-mail: murai@mail.sci.hokudai.ac.jp

Accepted 2006 July 20. Received 2006 July 20; in original form 2005 September 28

SUMMARY

We compute the synthetic seismograms of multiply scattered *SH* waves in 2-D elastic media with densely distributed parallel cracks. We assume randomly distributed cracks in a rectangular-bounded region, which simulate a cracked zone. The crack surfaces are assumed to be stress-free. When the incident wavelength is longer than the crack size, the delay in the arrival of the primary wave is observed at stations beyond the cracked zone and the amplitude of the primary wave is amplified in the cracked zone in the synthetic seismograms. This is because the cracked zone behaves as a low velocity and soft material to the incident long-wavelength wave due to the crack distribution. When the half-wavelength of the incident wave is shorter than the crack length, the scattered waves are clearly observed in the synthetic seismograms and the amplitude of the primary wave is largely attenuated beyond the cracked zone. The calculated attenuation coefficient Q^{-1} of the primary wave is directly proportional to the crack density in the range of $\nu a^2 \leq 0.1$, where ν and a are the number density and half the length of cracks, respectively. This is consistent with that obtained by a stochastic analysis based on Foldy's approximation. A periodic distribution of cracks in a zone is considered as an utterly different model in order to investigate the effect of spatial distributions on the attenuation and dispersion of seismic waves. When cracks are distributed densely, the values of Q^{-1} for the periodic crack distribution appear to differ from those for the random distribution of cracks in the low wavenumber range. This suggests that the effect of multiple interactions among densely distributed cracks depends on not only the density but also the spatial distribution of cracks at low wavenumbers. The calculated phase velocity of the primary wave is consistent with that from the stochastic analysis in the range of $\nu a^2 \leq 0.1$ and does not depend on the spatial distribution of cracks. This suggests that the multiple crack interactions have a smaller effect to the phase velocity. Therefore, the crack density can be estimated from the values of the phase velocity for the cases of densely distributed cracks even if the effect of the multiple crack interactions is not considered. We can clearly observe the reflected waves in the synthetic seismograms. The elastic constant of a single anisotropic layer equivalent to the cracked zone is derived from the crack density at the long-wavelength limit. The reflection coefficients calculated from the synthetic seismograms are consistent with those of the anisotropic layer calculated from its elastic constants and thickness in low wavenumber range. This means that a fracture zone distributed parallel cracks is considered as an anisotropic layer for long incident wavelengths. Therefore, the elastic constants, crack density and the thickness of the fracture zone can be estimated from the frequency dependence of the reflection coefficients for long incident wavelengths. On the contrary the wavenumber dependence of the reflection coefficients cannot be explained theoretically in the high wavenumber range.

Key words: attenuation, cracked media, fracture zone, scattering, seismic anisotropy, synthetic seismograms.

1 INTRODUCTION

It is known that the Earth's crust is permeated by large numbers of cracks. In particular, the presence of densely distributed cracks is revealed in fault zones. Major crustal faults are not discrete planar faults but form fault zones. In general, a fault zone consists of several fault segments (e.g. Tchalenko 1970; Tchalenko & Berberian 1975). Each fault segment contains a great number of cracks on a

smaller scale. It is also revealed from seismic observations, such as shear wave splitting (Leary *et al.* 1987) and *P*-wave polarization anomalies (Li *et al.* 1987), that a fault zone is characterized as a zone of densely distributed cracks aligned parallel to the fault plane. Televiewer observations in boreholes also reveal the presence of distribution of parallel cracks within fault zones (Leary *et al.* 1987; Malin *et al.* 1988). Moreover it is shown from the KTB deep drilling and reflection experiments that the continental upper crust is highly fractured and that most of the reflected waves come from fracture zones or faults (Emmermann & Lauterjung 1997).

Cracks generally cause scattering for incident elastic waves, and dispersion and attenuation occur as a result. It is important to investigate dispersion and attenuation of elastic waves caused by distributed cracks for the prediction of large earthquakes. It is theoretically shown by Yamashita & Knopoff (1989, 1992) that large earthquakes are caused by the abrupt coalescence of pre-existing cracks; the crack distribution changes temporally in the crack coalescence process. If we can estimate the temporal variation of crack distribution from the observation of scattered waves, we may be able to monitor the earthquake preparation process.

Statistical elastic properties of media with distributed cracks have been studied intensively on the assumption of low wavenumber approximation (e.g. Hudson 1980, 1981). The importance of crack interactions has been investigated for the static case. Kachanov (1992) calculated the effective Young's modulus for solids with either randomly oriented or parallel cracks and indicated that the approximation of non-interacting cracks is applicable to the domain of strong interactions. Davis & Knopoff (1995) calculated the shear modulus of solids containing randomly oriented antiplane cracks and found that the mean-field approximation in which the cracks do not interact is appropriate up to quite high crack densities. Kachanov (1992) inferred the underlying reason is that the competing effects of stress shielding and stress amplification cancel each other. In contrast to the above, Dahm & Becker (1998) calculated the shear modulus for highly fractured inplane cracks and indicated that crack interactions are important at high crack densities.

Another problem is a wavenumber dependence of the crack interactions. Muijres *et al.* (1998) calculated acoustic wave propagation in a 2-D medium with many small cracks and observed an apparent attenuation and a time delay with respect to the incident field. They still assumed the wavelength considerably longer than the crack length. It is, however, essential to assume a wide wavenumber range to estimate the sizes of cracks from seismic waves. Some authors theoretically treat elastic wave scattering by distributed cracks without the low wavenumber approximation (e.g. Kikuchi 1981a,b; Yamashita 1990; Kawahara & Yamashita 1992). They employ the idea of the mean wave formalism and the approximation introduced by Foldy (1945). This approximation neglects crack interactions, so that it is valid when the distribution density of the cracks is low. However, the crack interactions cannot be neglected in treating problems of scattering in a medium with densely distributed cracks, such as in a fault zone. Numerical approaches are useful in order to investigate the effects of crack interactions for a wide wavenumber range. Murai *et al.* (1995) rigorously treated multiple crack interactions by applying a boundary integral equation method (BIEM) to the crack scattering problem. They could not deal with large numbers of cracks because they faced the difficulty of core memory and CPU time limits. Kelner *et al.* (1999) proposed a method to consider a large number of cracks; they used a boundary element method where the Green's functions are computed by the discrete wavenumber method. However, they gave no attention to media with densely distributed cracks. Vlastos *et al.* (2003) treated densely distributed cracks by finite-difference methods and investigated effects of crack sizes and spatial distributions. However, they did not investigate the attenuation and dispersion quantitatively. Murai & Yamashita (1998) proposed a method to treat multiple scattering of elastic waves due to densely distributed parallel cracks efficiently for arbitrary wavenumbers.

In this paper, we investigate the attenuation and dispersion of *SH* waves propagating through a zone of randomly distributed parallel cracks. We use BIEM developed by Murai *et al.* (1995). We can compute scattered waves taking account of multiple interactions among large numbers of cracks by BIEM because a state of the art computer is now available; we treat about five times as many cracks as those in Murai *et al.* (1995). We assume up to extremely high crack density, which has not been treated for the dynamic case before. It is important to check the validity of the conventional methods quantitatively because the low crack density has been assumed in estimating the crack density (e.g. Leary *et al.* 1987; Li *et al.* 2001). The crack surfaces are assumed to be stress-free. We compute the displacement field in the wavenumber domain, and obtain the synthetic waveforms by the Fourier transform. Next we evaluate the attenuation and dispersion of *SH* waves due to crack scattering by the same procedure Murai *et al.* (1995) used. These results are compared with those in the long-wavelength limit and those obtained by Kawahara & Yamashita (1992), who assumed randomly homogeneous distribution of cracks and analysed a stochastic wave equation based on Foldy's (1945) approximation. In addition we assume an elastic medium with periodic distribution of cracks in a zone as an utterly different model for the highest crack density assumed in the present paper in order to investigate the effect of spatial distributions on the attenuation and dispersion of seismic waves. We use the method introduced by Murai & Yamashita (1998), which is simple enough and enables us to obtain the solution for the case of the periodic distribution of cracks. We show that the attenuation of incident waves is affected by both of the crack density and the spatial distributions for the low wavenumber ranges when the distribution density of the cracks becomes higher. Finally, we investigate the wavenumber dependence of reflection coefficients of the cracked zone. We show that a zone of densely distributed parallel cracks behaves as an anisotropic layer in the low wavenumber range. In contrast, the reflection coefficients fluctuate greatly among observation stations and their wavenumber dependence becomes far from that predicted theoretically in the high wavenumber range. We show it is possible to estimate the crack density and thickness of a cracked zone by fitting the reflection coefficients to those of an anisotropic layer for incident long-wavelength waves.

2 SPATIAL DISTRIBUTION OF CRACKS

We consider a 2-D isotropic homogeneous elastic medium with N cracks randomly distributed in a rectangular-bounded region (Fig. 1). All the cracks are assumed to have the same length $2a$ and the same strike direction, which coincides with the X-axis in the defined coordinate system (X, Y). The sides of the rectangular-bounded region have lengths of $68.0a$ and $13.6a$ in the X and Y directions, respectively. The length of the cracked region in the X direction is assumed to be five times of that in the Y direction in order to consider a zonal distribution of cracks. The statistical distribution of cracks is now assumed to be homogeneous and the number density ν is defined as $\nu = N/924.8a^2$. We determine the centre of each crack (p_j, q_j) $(j = 1, \ldots, N)$ by generating $2N$ uniform

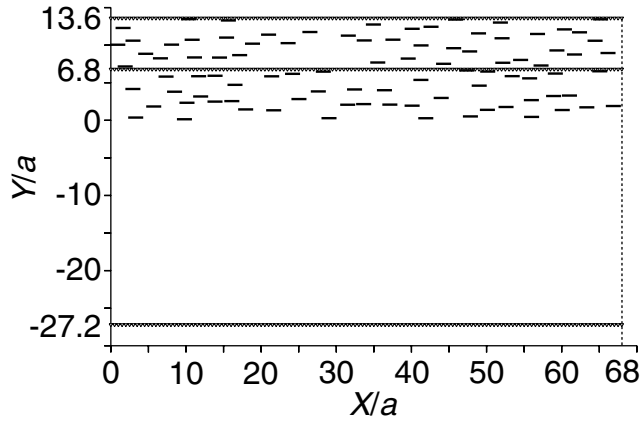

Figure 1. An example of the distribution of cracks and observation stations. 92 cracks are distributed in a rectangular-bounded region of sides $68.0a$ and $13.6a$ in the X and Y directions, respectively ($\nu a^2 = 0.1$). The rows of triangles denote the positions of the stations.

random numbers between 0 and 1, which are multiplied by $68.0a$ and $13.6a$ for p_j and q_j, respectively. If a centre of a crack is determined with a distance less than $2a$ from a centre of a neighbour, we revoke and determine it again by generating two more uniform random numbers.

A *SH* plane wave incident upon the lower boundary of the cracked region is assumed in the form

$$u_0(X, Y) = \exp[ik(X\cos\varphi + Y\sin\varphi)], \tag{1}$$

where i is the imaginary unit, k is the wavenumber and φ is the angle between the X-axis and the propagation direction of the incident plane wave. Here the time factor $\exp(-i\omega t)$ is omitted for brevity, where $\omega = k\beta$ and β is the shear wave velocity of the matrix.

All the crack surfaces are assumed to be stress-free. We assume $\nu a^2 = 0.05$, 0.075 and 0.1 and $\varphi = 90^\circ$ and 45°. The highest crack density 0.1 is larger than those assumed for the dynamic case before: 0.02 in Murai *et al.* (1995) and 0.075 in Kelner *et al.* (1999). We compute the synthetic seismograms by using the method employed by Murai *et al.* (1995). Observation stations are denoted by triangles in Fig. 1. 137 stations are located along each of the lines $Y = 13.6a$, $6.8a$ and $-27.2a$ in the range $0 \le X \le 68.0a$ with the interval of $0.5a$; note that the stations at $Y = 6.8a$ are located at the centre of the cracked zone.

3 SYNTHETIC SEISMOGRAMS

In this section, we compute the synthetic seismograms in the time domain. The seismograms in the time domain are obtained by Fourier transforming the solutions for 535 wavenumbers in the range from $ka = 0.01$ to 5.35. We use the Ricker wavelet as the time function of the incident waves. It is given by

$$s(t) = \frac{\beta k_c}{2\sqrt{\pi}}\left[\frac{1}{2} - \left(\frac{\beta k_c t}{2}\right)^2\right]\exp\left[-\left(\frac{\beta k_c t}{2}\right)^2\right], \tag{2}$$

whose spectrum is

$$S(k) = \frac{k^2}{k_c^2}\exp\left(-\frac{k^2}{k_c^2}\right), \tag{3}$$

where k_c is the characteristic (peak) wavenumber of the wavelet (see Fig. 2).

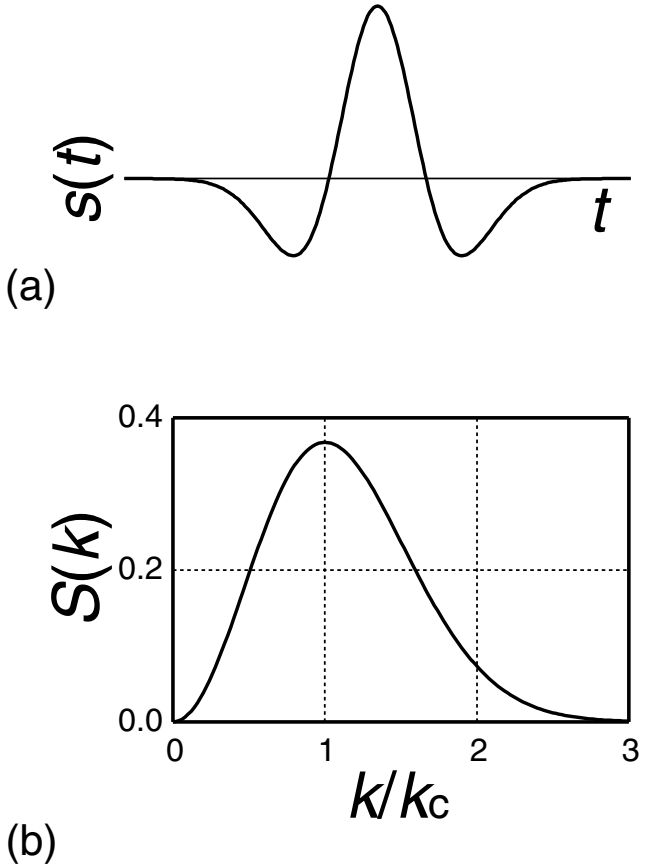

Figure 2. (a) Ricker wavelet time function and (b) its amplitude spectrum.

The synthetic displacement seismograms for the crack distribution in Fig. 1 are shown in Figs 3 and 5, where normal incidence of *SH* plane waves are assumed; the seismograms for the same $k_c a$ value are drawn in the same scale except that the later arrivals in Fig. 3(c) are drawn in the five times as large scale as others. In this model the crack density νa^2 is 0.1, which is the densest distribution of cracks assumed in this study. The characteristic non-dimensional wavenumber of the wavelets, $k_c a$, is assumed to be 0.25 in Fig. 3. The wavenumber corresponds to the characteristic wavelength, $\lambda_c = 2\pi/k_c$, of about $25.1a$, which is much longer than the crack size. The seismograms at the stations along the lines $Y = 13.6a$, $6.8a$ and $-27.2a$ are shown in Figs 3(a), (b) and (c), respectively. These figures show that the scattered wave energy is relatively weak when the wavelength of the incident wave is longer than the crack size. The peak amplitude of the primary wave shows little attenuation in Fig. 3(a). The delay in the arrival of the primary wave is observed at stations beyond the cracked region, which is due to scattering by distributed cracks; note that the peak of the primary wave would arrive exactly at time $\beta t/a = 13.6$ when no crack existed. This is because the cracked zone behaves as a low-velocity zone due to the crack distribution. We can observe the effect at the ends of the crack distribution region; it is clearly seen that the time delay for the peak amplitude arrivals of the primary wave is smaller at the stations close to the ends of the crack distribution region. In Fig. 3(b) the peak amplitude of the primary wave is amplified at $Y = 6.8a$ in the cracked zone, which is clearly shown by the peak amplitudes of the primary wave normalized by that of the incident wave (solid curve in Fig. 4); the normalized amplitudes are larger than unity at almost all the stations. This is because the cracked zone also behaves

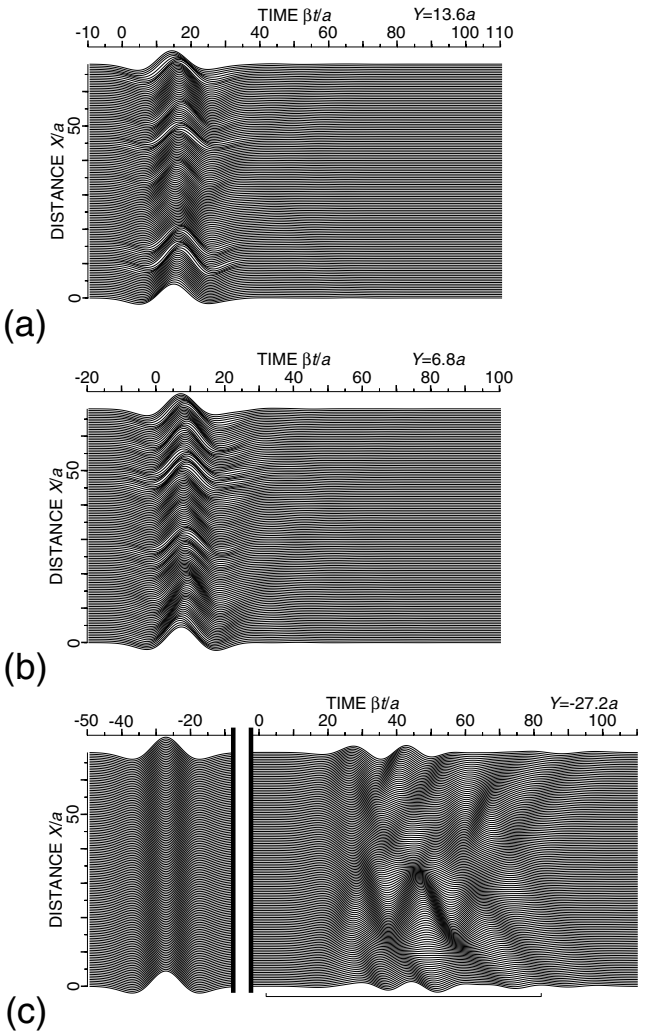

Figure 3. Synthetic displacement seismograms for the crack distribution in Fig. 1. $\varphi = 90^\circ$ and $k_c a = 0.25$ are assumed. The seismograms recorded at the stations along the lines $Y = 13.6a$, $6.8a$ and $-27.2a$ are shown in (a), (b) and (c), respectively. The bracket in (c) denotes a time window of $80\beta/a$ to calculate the reflection coefficient plotted in Fig. 9(a).

as a soft material to the incident long-wavelength wave due to the crack distribution. However, this phenomenon does not mean that the amplitude is increasing with the propagating distance. It is true that the amplitudes are larger in the cracked zone than that of the incident wave, but it is attenuated as shown by the broken curve in Fig. 4 after the wave propagates in the cracked zone. Here the normalized amplitudes are larger than unity at the stations close to the ends of the crack distribution region. This is the effect at the ends of the crack distribution region, which will be stated for details in the next section. We can observe the reflected waves in Fig. 3(c). The first peak of the wave reflected at the lower boundary of the cracked region arrives at time around $\beta t/a = 27.2$ and the opposite phase reflected at the upper boundary arrives at around $\beta t/a = 50 \sim 60$. The duration of the reflected waves is almost the same as the two way traveltime of the incident wave propagating within the cracked zone.

The seismograms for $k_c a = 2.0$ corresponding to $\lambda_c = 3.14a$ at the stations along the lines $Y = 13.6a$, $6.8a$ and $-27.2a$ are shown in Figs 5(a), (b) and (c), respectively. We can clearly observe the scattered waves when the half-wavelength of the incident wave is

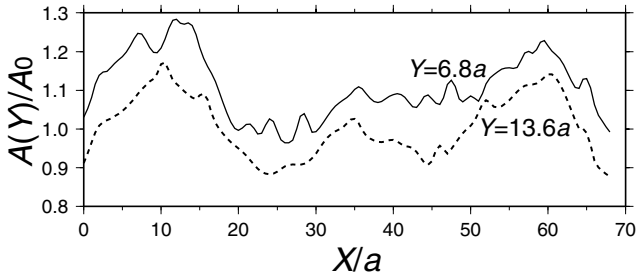

Figure 4. The peak amplitudes of the primary wave shown in Figs 3(a) and (b) normalized by that of the incident wave, where A_0 and $A(Y)$ are the peak amplitudes of the incident wave and the primary waves at the stations, respectively. The solid and broken curves denote the normalized amplitudes at the stations along the lines $Y = 6.8a$ and $13.6a$, respectively.

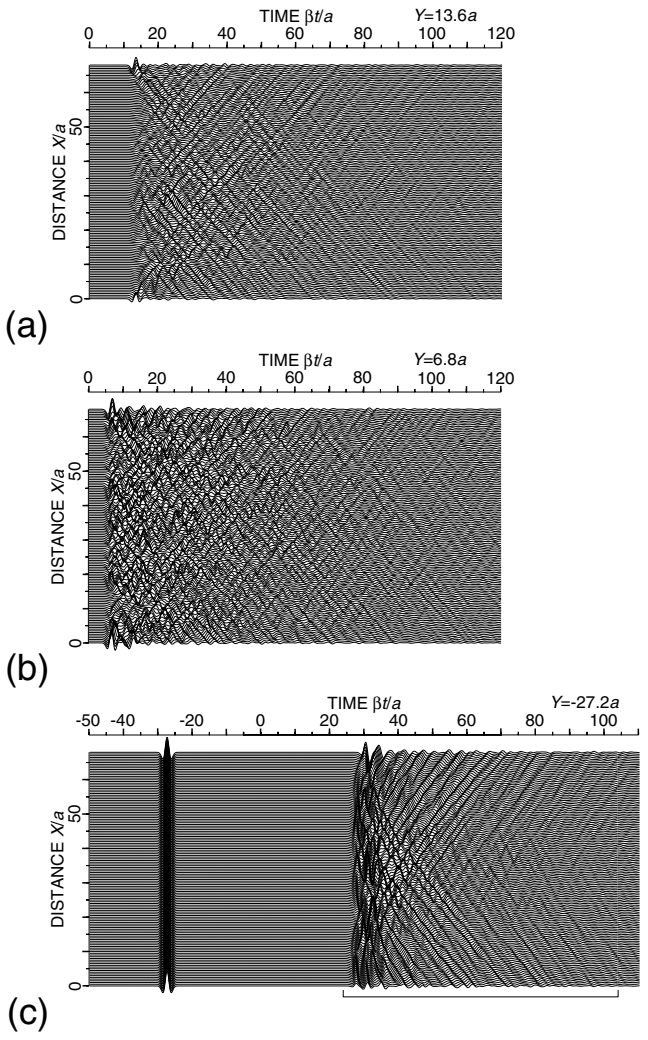

Figure 5. The same as in Fig. 3 except for $k_c a = 2.0$.

shorter than the crack length. The fluctuations are larger in both arrival times and amplitudes in Fig. 5 than in Fig. 3; the standard deviations of the fluctuations in arrival times and amplitudes of the primary peak in Fig. 3(a) are 0.57 and 0.017, respectively, while 1.1 and 0.15 in Fig. 5(a), respectively. The peak amplitude of the primary wave is largely attenuated as observed in Fig. 5(a). This phenomenon means that the energy of the primary waves flows into

the coda portion due to scattering. It is also shown in Fig. 5(a) that the time delay of the primary wave is smaller than that shown in Fig. 3(a). The effects at the ends of the crack distribution region are as clear as in Fig. 3(a); it is clearly seen that the amplitude is larger at the stations close to the ends of the crack distribution region in addition to the smaller time delay for the peak amplitude arrivals of the primary wave. There exist 'shadows' in Fig. 5(b) at stations immediately above cracks, that is, the stations in the ranges $10a \leq X \leq 15a$ and $50a \leq X \leq 60a$ (see Fig. 1). This phenomenon can be understood as the high-wavenumber behaviour of wave propagation described by the geometrical ray theory (Červený 2001, pp. 612–613); no rays penetrate through crack surfaces by the ray theoretical approach. The amplitudes of the reflected waves are larger in Fig. 5(c) than in Fig. 3(c). This is because higher-wavenumber energy is more abundant in the waves scattered from the cracked zone as in Figs 5(a) and (b). The duration of the reflected waves has a tendency to increase for higher crack density at high wavenumbers.

4 ATTENUATION COEFFICIENT Q^{-1} AND PHASE VELOCITY v

It was shown in the preceding section that the distributed cracks generally cause attenuation for the primary wave and the time delay for the peak amplitude arrivals. We now quantitatively investigate the propagation of the primary wave in the cracked region. In other words, we evaluate the attenuation coefficient Q^{-1} and the phase velocity v.

We apply a Butterworth bandpass filter with octave bandwidth to the synthetic seismograms for the stations beyond the cracked zone. We estimate Q^{-1} and v from the peak amplitude of the primary wave and its traveltime from $Y = 0$ to $Y = h$ for four non-dimensional wavenumbers, $ka = 0.5$, 1.0, 2.0 and 4.0 by applying the same procedure as Murai *et al.* (1995), where h is the width of the cracked zone, that is, $13.6a$. These wavenumbers correspond to wavelengths of about $12.6a$, $6.28a$, $3.14a$ and $1.57a$, respectively. Q^{-1} and v are obtained at each station by using the following equations:

$$A(h) = A_0 \exp\left(-\frac{k\beta h}{2vQ\sin\varphi}\right), \tag{4}$$

$$\frac{v}{\beta} = \frac{t_s}{t_s^*}, \tag{5}$$

where A_0 is the peak amplitude of the incident wave, $t_s = h/\beta \sin\varphi$ is the traveltime of the primary peak from $Y = 0$ to $Y = h$ without cracks, $A(h)$ and $t_s^* = h/v\sin\varphi$ are the peak amplitude of the primary wave at $Y = h$ and its traveltime from $Y = 0$ to $Y = h$, respectively. The width of the cracked zones, which is $h = 13.6a$, is assumed to be longer than $12.6a$ that is the longest wavelength of the lowest wavenumber, that is, $ka = 0.5$, assumed here.

Now the effects at the ends of the crack distribution region, which are clearly seen in the preceding section, have to be avoided. We can find out which stations suffer from such effects by the following procedure. We consider an elastic medium with periodic distribution of cracks in a zone as illustrated in Fig. 6(a). The crack density νa^2 is 0.1 which is the same as that in Fig. 1. The synthetic seismograms can be computed by the same procedure as in the preceding section. In addition we can compute synthetic seismograms for the same periodic distribution of cracks except for the infinite distribution in the X direction by the method introduced by Murai & Yamashita (1998). The effects at the ends of the crack distribution region can be seen by comparing both results. Fig. 6(b) shows comparison of the peak amplitudes of the primary wave at $Y = 13.6a$ normalized by those of the incident wave, where $\varphi = 90^\circ$ and $k_c a = 0.5$ are assumed. The effects are clearly seen at the stations whose distance from the ends of the crack distribution region is less than $12.6a$, which is the characteristic wavelength of the incident Ricker wavelet. In a similar way, we select stations whose X-coordinates are in the range $(h\cos\varphi + 12.6a)/\sin\varphi \leq X \leq L - 12.6a$ in the calculation of Q^{-1} and v, where L is the length of the cracked zone in the X direction, that is, $68.0a$; note that $12.6a$ is the longest wavelength to estimate Q^{-1} and v. We calculate the mean values and the standard deviations of Q^{-1} and v from the calculated values of $A(h)$ and t_s^* through eqs (4) and (5).

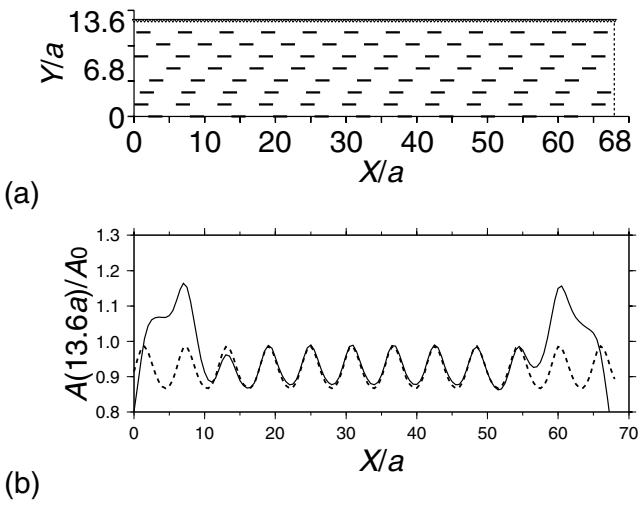

Figure 6. (a) Periodic distribution of cracks in a zone and observation stations considered to investigate the effects at the ends of the crack distribution region. The crack spacing is $5.88a$ and $1.7a$ in the X and Y directions, respectively ($\nu a^2 = 0.1$). The row of triangles denotes the positions of the stations. (b) The peak amplitudes of the primary wave at the stations in (a) normalized by that of the incident wave. $\varphi = 90^\circ$ and $k_c a = 0.5$ are assumed. The solid curve denotes the normalized amplitudes for the crack distribution in (a), while the broken curve denotes those for the same crack distribution as (a) except for the infinite distribution in the X direction.

The wavenumber dependence of Q^{-1} for the assumed crack density is plotted in Fig. 7 with open circles. Each symbol stands for the mean value obtained by averaging over the stations; the error bar denotes the standard deviation. Figs 7(a), (b) and (c) show the values of Q^{-1} in the case of normal incidence ($\varphi = 90^\circ$) for the crack distribution models with the density $\nu a^2 = 0.05$, 0.075 and 0.1, respectively. These figures show that Q^{-1} takes the peak value near $ka = 1 \sim 2$; this means that the crack scattering is dominant when the half-wavelength of the incident wave is close to the crack length. This property is consistent with previous studies concerning attenuation of elastic waves in media with cracks or cavities (Benites *et al.* 1992; Murai *et al.* 1995; Kelner *et al.* 1999). The values of Q^{-1} obtained by Kawahara & Yamashita (1992) based on Foldy's (1945) approximation are plotted as solid curves in Fig. 7. We note that our results agree well with theirs even for the case of the high crack density, that is, $\nu a^2 = 0.1$. Fig. 7(d) shows the values of Q^{-1} for the case of oblique incidence ($\varphi = 45^\circ$) and $\nu a^2 = 0.1$. In this figure the values of Q^{-1} are smaller than those for the case of normal incidence shown in Fig. 7(c). This can be explained from the characteristics of *SH*-type motion and the propagation direction of the incident wave represented by eq. (1); there is a smaller resistance to the incident wave for smaller φ.

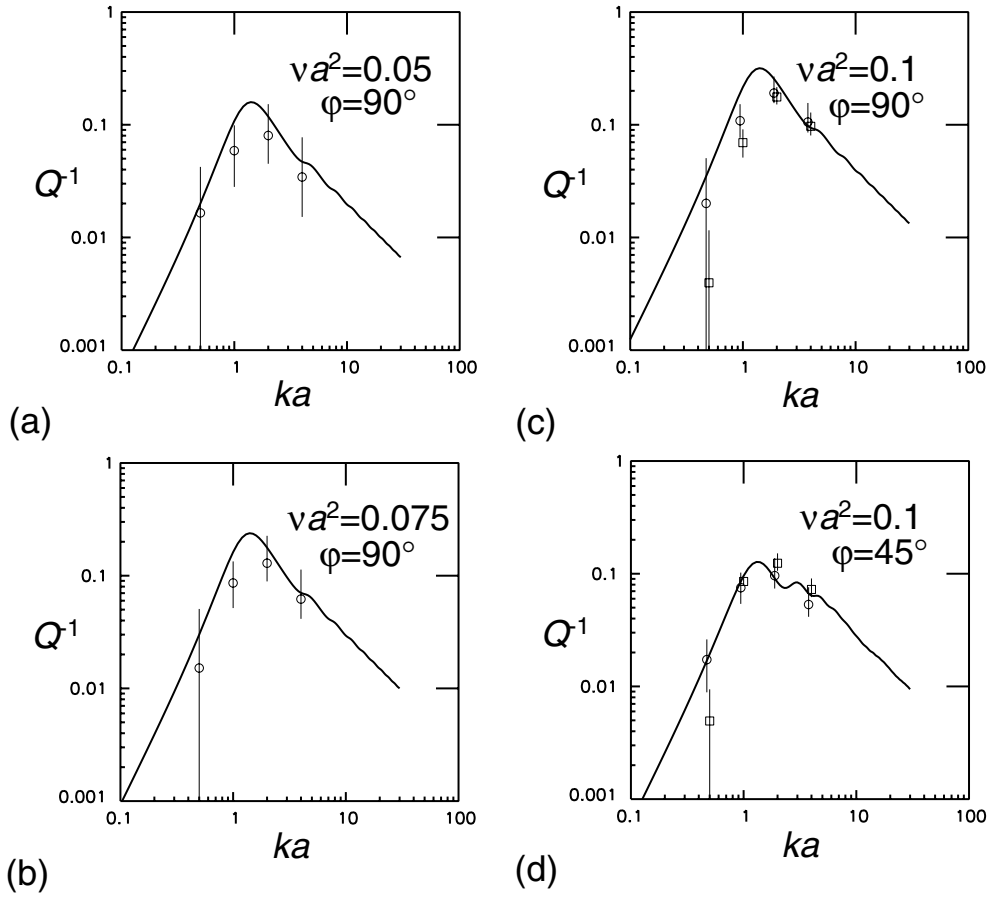

Figure 7. The wavenumber dependence of Q^{-1}. Each symbol represents the mean value, and the error bar denotes the standard deviation. The open circles correspond to the crack distribution models of the same rectangular-bounded region as in Fig. 1 for each crack density. The open squares in (c) and (d) correspond to the model of the periodic distribution of cracks shown in Fig. 6(a) except for the infinite distribution in the X direction. The results obtained by Kawahara & Yamashita (1992) are also plotted, as solid curves (reproduced with permission from Birkhäuser Verlag). (a) Q^{-1} for the case of $\nu a^2 = 0.05$ and $\varphi = 90^\circ$. (b) Q^{-1} for the case of $\nu a^2 = 0.075$ and $\varphi = 90^\circ$. (c) Q^{-1} for the case of $\nu a^2 = 0.1$ and $\varphi = 90^\circ$. (d) Q^{-1} for the case of $\nu a^2 = 0.1$ and $\varphi = 45^\circ$.

Next we investigate the wavenumber dependence of the phase velocity v. The values of $(\beta - v)/\beta$ are plotted in Fig. 8 with the open circles for the assumed crack density. Each symbol represents the mean value obtained by averaging over the stations; the error bar denotes the standard deviation. Figs 8(a), (b) and (c) show the values of $(\beta - v)/\beta$ in the case of normal incidence ($\varphi = 90^\circ$) for the crack distribution models with the density $\nu a^2 = 0.05$, 0.075 and 0.1, respectively. Fig. 8(d) shows the values of $(\beta - v)/\beta$ for the case of oblique incidence ($\varphi = 45^\circ$) and $\nu a^2 = 0.1$. The standard deviations are large at $ka = 2.0$ and 4.0. This is because the time delay of the primary wave is small and the deviations are relatively large at the high wavenumber as described in the preceding section. Kawahara & Yamashita's (1992) results are plotted by solid curves in Fig. 8. This figure shows our results agree well with theirs even for the case of densely distributed cracks; $\beta - v$ is directly proportional to the crack density to the high crack density, that is, $\nu a^2 = 0.1$. This suggests the multiple crack interactions have a smaller effect to the phase velocity. Therefore, the crack density can be estimated from the values of the phase velocity for the cases of densely distributed cracks even if the effect of the multiple crack interactions is not considered.

Moreover we compare our results with those predicted by the theory of homogeneous media equivalent to a fractured material for long incident wavelength. The velocity at the low wavenumber limit is given to the first order in νa^2 by Ohno *et al.* (2001) as

$$(\beta - v)/\beta = \pi \nu a^2 \sin^2 \varphi / 2. \tag{6}$$

Their values are plotted by the broken lines in Fig. 8. In the low wavenumber domain, our results are very close to the values obtained on the assumption of low wavenumber approximation. This result is in agreement with the previous study by Kelner *et al.* (1999). Inversely we try to estimate the crack density by using eq. (6) from the phase velocities obtained above for the case of $\nu a^2 = 0.1$. We obtained the values of $(\beta - v)/\beta$ as 0.164 and 0.090 for $\varphi = 90^\circ$ and 45°, respectively for $ka = 0.5$. When these values are substituted into eq. (6), the crack density is estimated as $\nu a^2 = 0.10$ and 0.11 for $\varphi = 90^\circ$ and 45°, respectively. These values are very close to the correct density of 0.1. This suggests the low wavenumber approximation is good enough even for the case of $\nu a^2 = 0.1$.

Finally, we investigate the wavenumber dependence of Q^{-1} and v for the case of the periodic distribution of cracks shown in Fig. 6(a) as an utterly different model in order to investigate the effect of spatial distributions on the attenuation and dispersion of seismic waves. The crack density νa^2 is 0.1, which is the highest density assumed in the present paper. We use the method introduced by Murai & Yamashita (1998) to compute the synthetic seismograms for the infinite crack distribution in the X direction. The wavenumber domain solutions are calculated for the same wavenumbers for the same stations as in

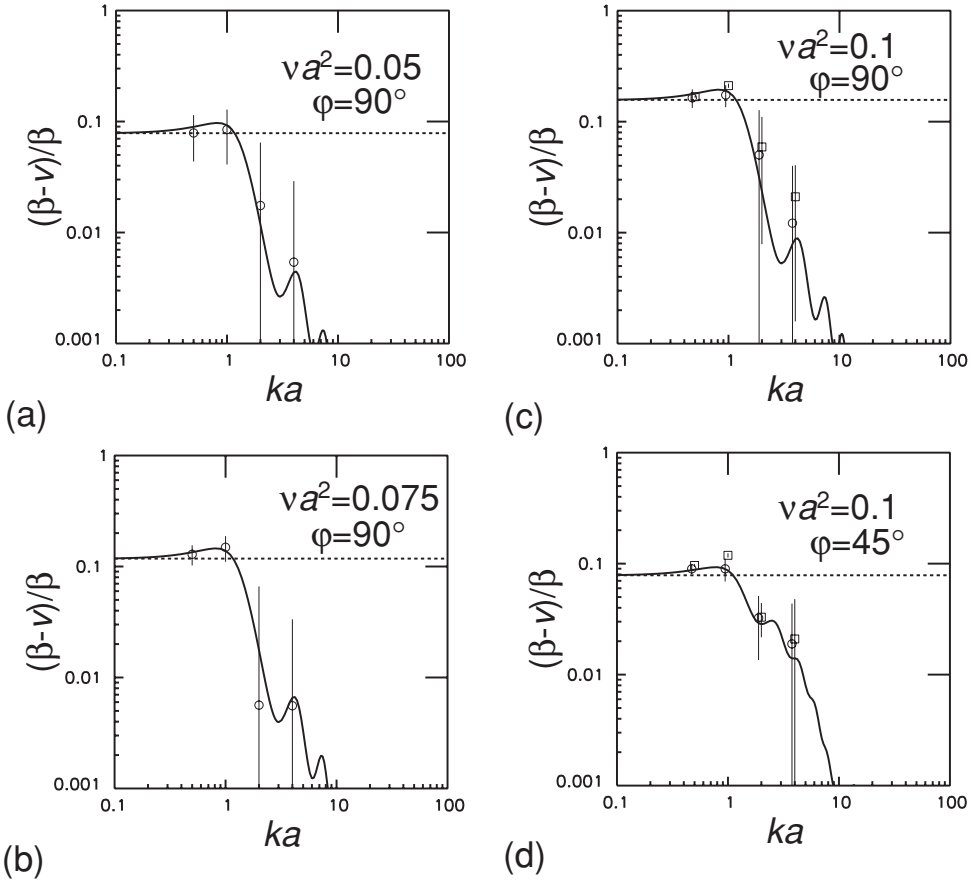

Figure 8. The wavenumber dependence of $(\beta - v)/\beta$ for the same cases as in Fig. 7. The broken lines denote the values at the low wavenumber limit given by Ohno *et al.* (2001).

the case of the random distribution of cracks. The values of Q^{-1} and $(\beta - v)/\beta$ for the periodic distribution of cracks are also plotted as open squares in Figs 7(c) and (d), and Figs 8(c) and (d), respectively. We assume normal incidence to the crack surfaces ($\varphi = 90^\circ$) in Figs 7(c) and 8(c), and oblique incidence ($\varphi = 45^\circ$) in Figs 7(d) and 8(d), respectively. Figs 7(c) and (d) show the values of Q^{-1} for the periodic crack distribution seem to differ from those for the random distribution of cracks at $ka = 0.5$. This suggests that the effect of multiple interactions among densely distributed cracks depends on not only the density but also the spatial distribution of cracks at low wavenumbers. On the other hand Figs 8(c) and (d) show that the values of $(\beta - v)/\beta$ do not depend on the spatial distribution of cracks. This suggests that the multiple crack interactions have a smaller effect to the phase velocity as stated before and that the values of $\beta - v$ depend only on the crack density.

5 REFLECTION COEFFICIENTS

In the present paper, we assume a zonal distribution of parallel cracks, which is considered to be a fracture zone. It was shown in Figs 3(c) and 5(c) that the cracked zone excites the reflected waves. In general it is possible to estimate an internal structure of a fracture zone by investigating a frequency dependence of reflection coefficients. This is the same analysis as that for estimating an internal structure of a reflected body in a mid-crust (e.g. Ake & Sanford 1988; Matsumoto & Hasegawa 1996). We investigate the wavenumber dependence of reflection coefficients of the cracked zone in this section. We assume the randomly distributed cracks with the density $\nu a^2 = 0.1$ as illustrated in Fig. 1.

The reflection coefficients are calculated by the following procedure. First, we compute the synthetic seismograms at stations in the incidence media with the Ricker wavelet as the source time function; we assume the Ricker wavelets whose $k_c a$ are 0.25, 0.5, 1.0, 2.0 and 4.0. The stations are located along the line $Y = -27.2a$ in the range $0 \le X \le 68.0a$ with the interval of $0.5a$ (Fig. 1). Next, we calculate the amplitude spectrum for each Ricker wavelet source time function in a time window of $80\beta/a$ including the reflected waves using a cosine type window with $8\beta/a$ edge length. The spectral window is shown in Figs 3(c) and 5(c) for the case of normal incidence ($\varphi = 90^\circ$) as an example. Finally, the amplitude spectrum for each Ricker wavelet is normalized by that of each source time function to eliminate the contribution of source spectra. The reflection coefficient for each Ricker wavelet is calculated for the range of $0.09/a \le k \le 4\,k_c/3$ for $k_c a = 0.25$, and $2\,k_c/3 \le k \le 4\,k_c/3$ for $k_c a = 0.5$, 1.0, 2.0 and 4.0, respectively. Here we find which stations should be selected for calculation of the reflection coefficients in order to avoid the possible effects at the ends of the crack distribution region by the same way as for estimation of Q^{-1} and v in the preceding section. We consider the periodic distribution of cracks shown in Fig. 6(a) and compare the reflection coefficients with those for the case of the infinite distribution in the X direction. We select stations whose X-coordinates are in the range $(-Y_s \cos\varphi + 12.6a)/\sin\varphi \le X \le \min\{L - (Y_s \cos\varphi + 12.6a)/\sin\varphi,\ L\}$, where Y_s is the Y-coordinate of the observation stations to calculate the reflection coefficients. The reflection coefficients are plotted in Fig. 9.

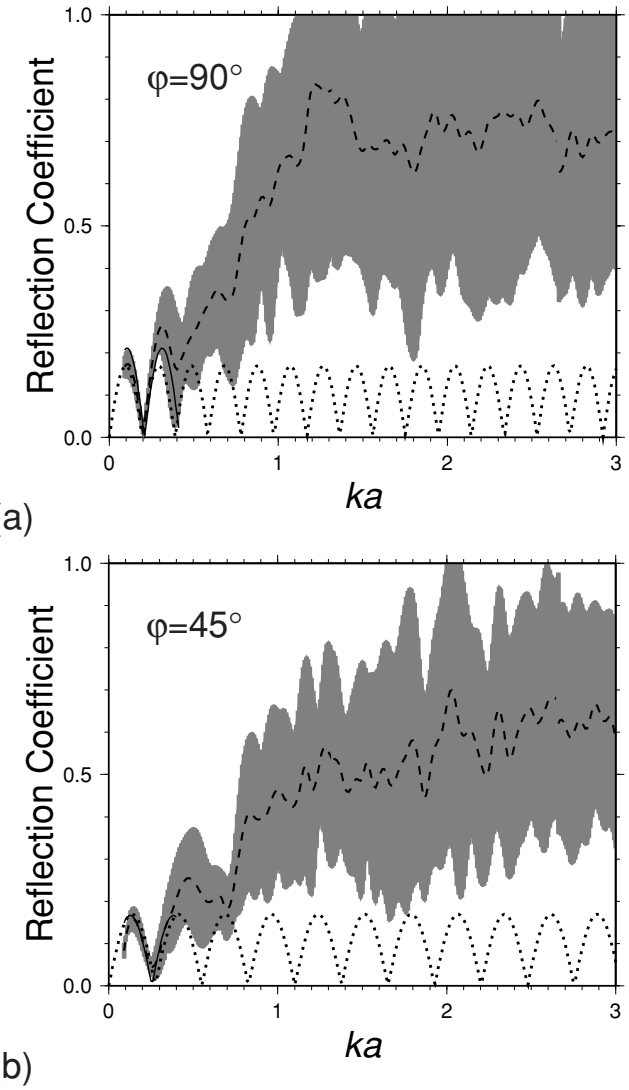

Figure 9. The reflection coefficients calculated from the synthetic seismograms for the crack distribution model shown in Fig. 1. Each broken curve represents the mean value, and each grey-shaded range denotes the standard deviation. The reflection coefficient calculated for the best-fit model of the single low-velocity layer is also plotted by the solid curve for the wavenumber range used in fitting in each of (a) and (b). The dotted curves are the reflection coefficients calculated for the single anisotropic layer of $c_{2323} = 0.711\mu$, $c_{1212} = \mu$, $c_{1223} = 0$ and $w = 13.6a$ which is considered to be equivalent to the cracked zone illustrated in Fig. 1. $\varphi = 90^\circ$ and 45° are assumed in (a) and (b), respectively.

Each broken curve stands for the mean value obtained by averaging over the stations and the grey-shaded range denotes one standard deviation.

Fig. 9(a) shows the reflection coefficient for the case of normal incidence. This figure shows that the reflection coefficient has peaks periodically for $ka \leq 0.4$. The wavenumber dependence is identical with that of a single low-velocity layer (e.g. Ake & Sanford 1988; Watanabe 1993; Matsumoto & Hasegawa 1996); peaks of the reflection coefficient appear when $w = (\lambda/4)(2m - 1)$, where w is the thickness of the low-velocity layer, λ is the wavelength and $m = 1, 2, \ldots$ (Fuchs 1969). Such wavenumber dependence is explained by the interference of resonated waves in a layer (Ake & Sanford 1988). We now try to estimate the velocity and thickness of the fracture zone by fitting the reflection coefficient to that of a single low-velocity layer in the range of $0.09 \leq ka \leq 0.4$. The best-fit model is estimated as $v/\beta = 0.807$ and $w = 12.2a$ and the calculated reflection coefficient from the single low-velocity layer model is plotted by the solid curve in Fig. 9(a). In the preceding section, v/β of this cracked zone with the width of $13.6a$ is estimated to be 0.832 for $ka = 0.5$. We find the velocity and thickness of the fracture zone can be estimated correctly from the wavenumber dependence of reflection coefficient in the low wavenumber range for the case of normal incidence. On the contrary the periodical behaviour of the reflection coefficient is lost in the high wavenumber range. The mean value seems to be almost constant for $ka > 1.0$ although the error range becomes very large. This is because the coherency of the wavefield disappears due to scattering and the interference does not occur.

Next, we consider a case of oblique incidence. A broken curve in Fig. 9(b) shows the reflection coefficient for the case of $\varphi = 45^\circ$. This figure shows the periodical behaviour of the reflection coefficient for $ka \leq 0.4$ as Fig. 9(a). We estimate the velocity and thickness of the fracture zone by the same procedure as for the case of normal incidence. The best-fit model is estimated as $v/\beta = 0.682$ and $w = 9.59a$ and the calculated reflection coefficient from the single low-velocity layer model is plotted by the solid curve in Fig. 9(b). The velocity structure is not estimated correctly; it is obvious that the width is underestimated. Moreover the velocity is also underestimated by the analysis of the reflection coefficient for the case of oblique incidence; v/β of this cracked zone model is estimated to be 0.910 for $ka = 0.5$ in the preceding section. Such a misestimate for the oblique incidence is considered to be caused by seismic anisotropy of parallel cracks. The wavenumber dependence is similar to that for the case of normal incidence in the high wavenumber range; the mean value seems to be almost constant for $ka > 1.0$ but somewhat smaller than that in Fig. 9(a) although the error range is very large. The smaller amplitudes of the reflected waves can be explained from the characteristics of *SH*-type motion; there is a smaller resistance to the incident wave represented by eq. (1) for smaller φ as stated in the preceding section. However, the reflection coefficient at the high wavenumber range does not seem to depend on the crack density.

We now consider reflection from a single anisotropic layer equivalent to the cracked zone. Appendix A gives the definition of the coordinate system and the computation of the reflection coefficients of an anisotropic layer and the *SH* wave velocity propagating in an anisotropic medium. Because the single anisotropic layer is equivalent to the cracked zone, v in eq. (6) equals to v_a in eq. (A26) at the low wavenumber limit. Therefore, the relation between the crack density νa^2 and the elastic constant c_{2323} is obtained from eqs (6) and (A26) as

$$\frac{c_{2323}}{\mu} = \frac{\sin^2\varphi(2 - \pi\nu a^2 \sin^2\varphi)^2}{4 - \cos^2\varphi(2 - \pi\nu a^2 \sin^2\varphi)^2}. \tag{7}$$

For $\nu a^2 = 0.1$ and $\varphi = 90^\circ$, the elastic constant of the anisotropic layer equivalent to the cracked zone illustrated in Fig. 1 is obtained as $c_{2323} = 0.711\mu$ from eq. (7). The reflection coefficients calculated for the single anisotropic layer with $c_{2323} = 0.711\ \mu$, $c_{1212} = \mu$, $c_{1223} = 0$ and $w = 13.6a$ are plotted by the dotted curves in Fig. 9. This figure shows that the reflection coefficients calculated from the synthetic seismograms agree well with those of the anisotropic layer in the range of $ka \leq 0.4$ for both the cases of $\varphi = 90^\circ$ and 45°. Therefore, a fracture zone distributed parallel cracks is considered as an anisotropic layer rather than a low-velocity layer and the elastic constants, crack density and the thickness of the

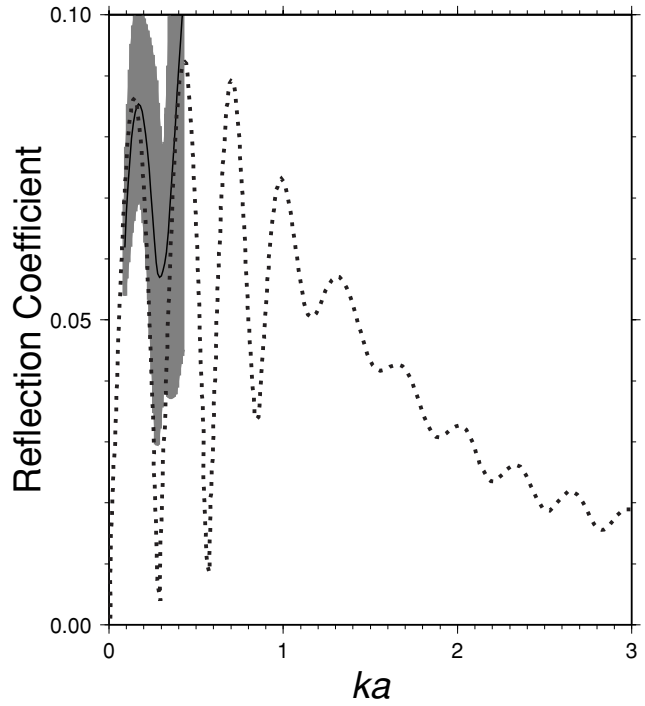

Figure 10. Comparison of the reflection coefficients calculated from the synthetic seismograms and given by Angel & Koba (1998) for the case of $w = 10a$, $\nu a^2 = 0.05$ and $\varphi = 90^\circ$. The solid curve denotes the mean value, and the grey-shaded range denotes the standard deviation calculated from the synthetic seismograms, while the broken curve denotes the solution by Angel & Koba (1998) (reproduced with permission from Elsevier).

fracture zone can be estimated from the frequency dependence of the reflection coefficients for long incident wavelengths. However, the reflection coefficients cannot be explained theoretically in the high wavenumber range.

Finally, we compare the reflection coefficient from our simulation with that theoretically obtained assuming Foldy's (1945) approximation. Kawahara & Yamashita (1992) and Angel & Koba (1998) derived reflection and transmission coefficients of a zone containing randomly distributed parallel cracks. Here Kawahara (2001) pointed out that there were errors in Kawahara & Yamashita's (1992) calculation because of the discrepancy between both the results. Therefore, we compare our result with that of Angel & Koba (1998). Fig. 10 shows the reflection coefficient for the case of $w = 10a$, $\nu a^2 = 0.05$ and $\varphi = 90^\circ$. This figure shows that both of the reflection coefficients agree well in the low wavenumber range but our result is not theoretically predicted in the high wavenumber range again.

6 DISCUSSION AND CONCLUSIONS

In this paper, we computed the synthetic seismograms of multiply scattered *SH* waves in 2-D elastic media with densely distributed parallel cracks. We assumed randomly distributed cracks in a rectangular-bounded region, which simulate a cracked zone. The crack surfaces are assumed to be stress-free. When the incident wavelength is longer than the crack size, the scattered wave energy is relatively weak. The delay in the arrival of the primary wave is observed at stations beyond the cracked zone and the amplitude of the primary wave is amplified in the cracked zone in the synthetic seismograms. This is because the cracked zone behaves as a low velocity and soft material to the incident long-wavelength wave due to the crack distribution. The work by Taniguchi & Oike (1984) is an example of the observational study of a behaviour of a fracture zone to incident long waves. They found that relative strains caused by teleseismic surface waves with periods less than one minute were larger across the fracture zones of the Yamasaki fault, southwestern Japan, than at the neighbouring bedrock. They explained this observation by the concept that a slight slip movement occurred along the fault surface. This feature is consistent with the assumption that small slips are caused across the crack surfaces by incident elastic waves in our model. When the half-wavelength of the incident wave is shorter than the crack length, the scattered waves are clearly observed in the synthetic seismograms and the amplitude of the primary wave is largely attenuated beyond the cracked zone.

Q^{-1} takes the peak value near $ka = 1 \sim 2$. This means that the crack scattering is dominant when the half-wavelength of the incident wave is close to the crack length. The values of Q^{-1} are directly proportional to the crack density in the range of $\nu a^2 \leq 0.1$ and consistent with those obtained by Kawahara & Yamashita (1992), who assumed Foldy's (1945) approximation. Because they employed the idea of the mean wave formalism, their values of Q^{-1} are those of the coherent wave motion scattered by randomly distributed cracks and do not mean the mean values obtained from the amplitudes of the single wave traces. However, coincidence of both results stands for the possibility that the values of Q^{-1} estimated from real seismic waves are explained by those obtained by using mean wave formalism even for the case of densely distributed cracks. In addition we assume the case of the periodic distribution of cracks in a zone as an utterly different model in order to investigate the effect of spatial distributions on the attenuation and dispersion of seismic waves. When cracks are distributed densely ($\nu a^2 = 0.1$), the values of Q^{-1} for the periodic crack distribution appear to differ from those for the random distribution of cracks in the low wavenumber ranges. This suggests that the effect of multiple interactions among densely distributed cracks depends on not only the density but also the spatial distribution of cracks at low wavenumbers. Keller (1964) indicated that the effective properties of cracked materials depend on the higher-order statistics of the crack distribution for higher crack densities, which is also summarized by Hudson & Knopoff (1989). Varadan *et al.* (1989) introduced the pair-correlation function as the higher-order statistics of the crack distribution. Although these studies suggest that the spatial distributions of cracks have an effect on the properties of wave propagation for higher crack densities, the wavenumber dependence is not referred because the size of the scatterer is assumed to be small compared to the incident wavelength. The present paper reveals that the effect of the spatial distributions of cracks is visible for Q^{-1} in the low wavenumber ranges. The accumulation of seismological measurements suggests that Q^{-1} of *S* waves in the lithosphere has a peak at around 0.5 Hz (e.g. Aki 1980). Considering our result that Q^{-1} is more sensitive to the spatial distribution of cracks at lower wavenumbers, it will be possible to detect the temporal variation of Q^{-1} associated with the earthquake occurrence process especially for Q^{-1} below the frequency of 0.5 Hz estimated in the epicentral region of imminent large earthquakes because the crack distribution changes temporally in the crack coalescence process before large earthquakes (Yamashita & Knopoff 1989, 1992).

On the other hand our results on $(\beta - v)/\beta$ are always consistent with Kawahara & Yamashita's (1992) in the range of $\nu a^2 \leq 0.1$ and do not depend on the spatial distribution of cracks. This suggests that the multiple crack interactions have a smaller effect to the phase velocity and that the value of $\beta - v$ is directly proportional to the crack density even for the case of densely distributed cracks.

Although this conclusion was indicated for the static case by the previous works (Kachanov 1992; Davis & Knopoff 1995), it is revealed to be applicable for a wide wavenumber range in this paper. Therefore, the crack density can be estimated from the values of the phase velocity for the cases of densely distributed cracks even if the effect of the multiple crack interactions is not considered.

We can clearly observe the reflected waves in the synthetic seismograms. The wavenumber dependence of the reflection coefficients has peaks periodically in the low wavenumber range. The wavenumber dependence is identical with that of a single low-velocity layer and a cracked zone seems to be a low-velocity layer for incident long wavelengths. The velocity and thickness of the cracked zone are estimated by fitting the reflection coefficient to that of a single low-velocity layer. It is shown that the velocity structure is estimated correctly for the case of normal incidence. However, both the width and velocity are underestimated for the case of oblique incidence. Such a misestimate is considered to be caused by seismic anisotropy of parallel cracks. Therefore, it is possible to obtain a wrong structure from the analysis of the reflection coefficient if the fracture zone containing a number of parallel cracks is simply assumed as a low-velocity layer. Then we consider a single anisotropic layer equivalent to the cracked zone. The elastic constant of such an anisotropic medium is derived from the crack density at the long-wavelength limit. The reflection coefficients calculated from the synthetic seismograms are consistent with those of the anisotropic layer calculated from its elastic constants and thickness for both the cases of normal and oblique incidence. This means that a fracture zone distributed parallel cracks is considered as an anisotropic layer rather than a low-velocity layer for long incident wavelengths. Therefore, the elastic constants, crack density and the thickness of the fracture zone can be estimated from the frequency dependence of the reflection coefficients for long incident wavelengths. On the contrary the reflection coefficients are highly fluctuated station by station due to scattering and the periodical behaviour is lost in the high wavenumber range. The wavenumber dependence cannot be explained theoretically.

It is revealed from seismic observations that aligned cracks are densely distributed in a fault zone (Leary *et al.* 1987; Li *et al.* 1987). The crack density in a fault zone has been estimated on a basis of the static elastic properties of cracked media on the assumption of low wavenumber approximation (e.g. Leary *et al.* 1987). However, it is not possible to estimate the sizes of cracks based on such an assumption. In this paper, we investigate the elastic properties of media with densely distributed cracks in a wide wavenumber range so that the results obtained here will be the basis to estimate a dominant crack length in a fracture zone.

Some authors consider scattering by distribution of circular cracks in 3-D media. Gross & Zhang (1992), Zhang & Gross (1993) and Eriksson *et al.* (1995) calculated attenuation and dispersion of elastic waves propagating in a medium containing a random distribution of penny-shaped microcracks by using Foldy's (1945) theory. They assumed a dilute distribution of cracks and neglected the effects of crack interactions. On the other hand, Hudson (1980) and a series of papers (e.g. Hudson 1986; Hudson *et al.* 1996) studied statistical elastic properties of media with distributed circular cracks in taking account of the second-order crack-crack interactions on the assumption of long wavelength approximation. There exists no study on crack scattering in 3-D media in consideration of the crack interactions for a wide wavenumber range. Further study is required to extend the present computations to 3-D simulations in order to detect crack distributions and investigate the mechanical properties of cracked media from seismic waves.

In the present paper, we assume the stress-free boundary condition on the crack surfaces. However, the existence of fluid is more realistic in cracked media. Some literature treats seismic wave propagation through material containing partially saturated cracks and/or fluid-saturated porous media with cracks although the incident wavelength is still assumed to be long compared to the size of cracks (Hudson 1988; Pointer *et al.* 2000; Hudson *et al.* 2001). In such media fluid flow occurs either within cracks or between cracks or cracks into a porous matrix. It is indicated that the movement of interstitial fluids within a cracked solid can have a significant effect on attenuation and dispersion of seismic waves even for long wavelength propagating through the solid (Pointer *et al.* 2000). It is also a future work that the present computations will include the effects of fluid flow.

ACKNOWLEDGMENTS

I thank Prof. T. Yamashita for critically reading this manuscript and Dr J. Kawahara for providing the result of Kawahara & Yamashita (1992) and helpful discussions. I also thank Dr T. Saito and the anonymous reviewers for helpful comments. This study was partly supported by a Grant-in-Aid from the Ministry of Education, Science, Sports and Culture of Japan (project 11740249) and the Earthquake Research Institute (ERI), the University of Tokyo, cooperative research programs (1999-B-04, 2000-B-07 and 2003-B-04). For this study, I have used the computer systems of Earthquake Information Center of ERI.

REFERENCES

Ake, J.P. & Sanford, A.R., 1988. New evidence for the existence and internal structure of a thin layer of magma at mid-crustal depths near Socorro, New Mexico, *Bull. seism. Soc. Am.,* **78,** 1335–1359.

Aki, K., 1980. Attenuation of shear-waves in the lithosphere for frequencies from 0.05 to 25Hz, *Phys. Earth planet. Inter.,* **21,** 50–60.

Angel, Y.C. & Koba, Y.K., 1998. Complex-valued wavenumber, reflection and transmission in an elastic solid containing a cracked slab region, *Int. J. Solids Struct.,* **35,** 573–592.

Benites, R., Aki, K. & Yomogida, K., 1992. Multiple scattering of *SH* waves in 2-D media with many cavities, *Pageoph,* **138,** 353–390.

Červený, V., 2001. *Seismic Ray Theory*, Cambridge University Press, Cambridge.

Dahm, T. & Becker, Th., 1998. On the elastic and viscous properties of media containing strongly interacting in-plane cracks, *Pageoph,* **151,** 1–16.

Davis, P.M. & Knopoff, L., 1995. The elastic modulus of media containing strongly interacting antiplane cracks, *J. geophys. Res.,* **100,** 18253–18258.

Emmermann, R. & Lauterjung, J., 1997. The German Continental Deep Drilling Program KTB: overview and major results, *J. geophys. Res.,* **102,** 18179–18201.

Eriksson, A.S., Boström, A. & Datta, S.K., 1995. Ultrasonic wave propagation through a cracked solid, *Wave Motion,* **22,** 297–310.

Foldy, L.L., 1945. The multiple scattering of waves. I. General theory of isotropic scattering by randomly distributed scatterers, *Phys. Rev.,* **67,** 107–119.

Fuchs, K., 1969. On the properties of deep crustal reflectors, *J. Geophys.,* **35,** 133–149.

Gross, D. & Zhang, Ch., 1992. Wave propagation in damaged solids, *Int. J. Solids Struct.,* **29,** 1763–1779.

Hudson, J.A., 1980. Overall properties of a cracked solid, *Math. Proc. Camb. phil. Soc.,* **88,** 371–384.

Hudson, J.A., 1981. Wave speeds and attenuation of elastic waves in material containing cracks, *Geophys. J.R. astr. Soc.,* **64,** 133–150.

Hudson, J.A., 1986. A higher order approximation to the wave propagation constants for a cracked solid, *Geophys. J.R. astr. Soc.,* **87,** 265–274.

Hudson, J.A., 1988. Seismic wave propagation through material containing partially saturated cracks, *Geophys. J.,* **92,** 33–37.

Hudson, J.A., Liu, E. & Crampin, S., 1996. The mechanical properties of materials with interconnected cracks and pores, *Geophys. J. Int.,* **124,** 105–112.

Hudson, J.A. & Knopoff, L., 1989. Predicting the overall properties of composite materials with small-scale inclusions or cracks, *Pageoph,* **131,** 551–576.

Hudson, J.A., Pointer, T. & Liu, E., 2001. Effective-medium theories for fluid-saturated materials with aligned cracks, *Geophys. Prospect.,* **49,** 509–522.

Kachanov, M., 1992. Effective elastic properties of cracked solids: critical review of some basic concepts, *Appl. Mech. Rev.,* **45,** 304–335.

Kawahara, J., 2001. Wave-theoretical properties of cracked media, *Zisin 2,* **54,** 91–108 (in Japanese).

Kawahara, J. & Yamashita, T., 1992. Scattering of elastic waves by a fracture zone containing randomly distributed cracks, *Pageoph,* **139,** 121–144.

Keith, C.M. & Crampin, S., 1977. Seismic body waves in anisotropic media: reflection and refraction at a plane interface, *Geophys. J.R. astr. Soc.,* **49,** 181–208.

Keller, J.B., 1964. Stochastic equations and wave propagation in random media, *Proc. Symp. appl. Math.,* **16,** 145–170.

Kelner, S., Bouchon, M. & Coutant, O., 1999. Numerical simulation of the propagation of *P* waves in fractured media, *Geophys. J. Int.,* **137,** 197–206.

Kennett, B.L.N., 1984. Reflection operator methods for elastic waves II—composite regions and source problems, *Wave Motion,* **6,** 419–429.

Kikuchi, M., 1981a, Dispersion and attenuation of elastic waves due to multiple scattering from inclusions, *Phys. Earth planet. Inter.,* **25,** 159–162.

Kikuchi, M., 1981b, Dispersion and attenuation of elastic waves due to multiple scattering from cracks, *Phys. Earth planet. Inter.,* **27,** 100–105.

Leary, P.C., Li, Y.-G. & Aki, K., 1987. Observation and modelling of fault-zone fracture seismic anisotropy—I. *P*, *SV* and *SH* travel times, *Geophys. J.R. astr. Soc.,* **91,** 461–484.

Li, Y.-G., Chester, F.M. & Vidale, J.E., 2001. Shallow Seismic profiling of the exhumed Punchbowl fault zone, Southern California, *Bull. seism. Soc. Am.,* **91,** 1820–1830.

Li, Y.-G., Leary, P.C. & Aki, K., 1987. Observation and modelling of fault-zone fracture seismic anisotropy—II. *P*-wave polarization anomalies, *Geophys. J.R. astr. Soc.,* **91,** 485–492.

Malin, P.E., Waller, J.A., Borcherdt, R.D., Cranswick, E., Jensen, E.G. & Van Schaack, J., 1988. Vertical seismic profiling of Oroville microearthquakes: velocity spectra and particle motion as a function of depth, *Bull. seism. Soc. Am.,* **78,** 401–420.

Matsumoto, S. & Hasegawa, A., 1996. Distinct *S* wave reflector in the mid-crust beneath Nikko-Shirane volcano in the northeastern Japan arc, *J. geophys. Res.,* **101,** 3067–3083.

Muijres, G.J. H., Herman, G.C. & Bussink, P.G.J., 1998. Acoustic wave propagation in two-dimensional media containing small-scale heterogeneities, *Wave Motion,* **27,** 137–154.

Murai, Y., Kawahara, J. & Yamashita, T., 1995. Multiple scattering of *SH* waves in 2-D elastic media with distributed cracks, *Geophys. J. Int.,* **122,** 925–937.

Murai, Y. & Yamashita, T., 1998. Multiple scattering of *SH* waves by imperfectly bonded interfaces with inhomogeneous strengths, *Geophys. J. Int.,* **134,** 677–688.

Ohno, T., Kawahara, J. & Yomogida, K., 2001. Attenuation and dispersion of *SH* waves due to scattering by 2-D cavities, *Abstracts Jpn. Earth Planet. Sci. Joint Meet.,* Sr-P002.

Pointer, T., Liu, E. & Hudson, J.A., 2000. Seismic wave propagation in cracked porous media, *Geophys. J. Int.,* **142,** 199–231.

Taniguchi, K. & Oike, K., 1984. Behavior of fractured zones at the Yamasaki fault for teleseismic surface waves, *J. Phys. Earth,* **32,** 449–461.

Tchalenko, J.S., 1970. Similarities between shear zones of different magnitudes, *Geol. Soc. Am. Bull.,* **81,** 1625–1640.

Tchalenko, J.S. & Berberian, M., 1975. Dasht-e Bayaz fault, Iran: earthquake and earlier related structures in bed rock, *Geol. Soc. Am. Bull.,* **86,** 703–709.

Varadan, V.K., Ma, Y. & Varadan, V.V., 1989. Scattering and attenuation of elastic waves in random media, *Pageoph,* **131,** 577–603.

Vlastos, S., Liu, E., Main, I.G. & Li, X.-Y., 2003. Numerical simulation of wave propagation in media with discrete distributions of fractures: effects of fracture sizes and spatial distributions, *Geophys. J. Int.,* **152,** 649–668.

Watanabe, T., 1993. Effects of water and melt on seismic velocities and their application to characterization of seismic reflectors, *Geophys. Res. Lett.,* **20,** 2933–2936.

Yamashita, T., 1990. Attenuation and dispersion of *SH* waves due to scattering by randomly distributed cracks, *Pageoph,* **132,** 545–568.

Yamashita, T. & Knopoff, L., 1989. A model of foreshock occurrence, *Geophys. J.,* **96,** 389–399.

Yamashita, T. & Knopoff, L., 1992. Model for intermediate-term precursory clustering of earthquakes, *J. geophys. Res.,* **97,** 19873–19879.

Zhang, Ch. & Gross, D., 1993. Wave attenuation and dispersion in randomly cracked solids—II. Penny-shaped cracks, *Int. J. Engng. Sci.,* **31,** 859–872.

APPENDIX A: REFLECTION AND TRANSMISSION COEFFICIENTS AND *SH* WAVE VELOCITY OF AN ANISOTROPIC LAYER

We derive the reflection and transmission coefficients of a 2-D anisotropic layer according to Keith & Crampin (1977). We consider an anisotropic medium equivalent to the cracked zone shown in Fig. 1 and define the coordinate system as shown in Fig. A1, where the X_1 axis is assumed to be parallel to the crack surfaces and a *SH* plane wave propagates in the X_1 direction with the velocity β which is the shear wave velocity of the isotropic medium. A *SH* plane wave incident upon the lower boundary of the anisotropic medium is assumed in the form

$$u_{02}(X_1, X_3) = \exp[-i\omega(t - X_1 \cos\varphi/\beta - X_3 \sin\varphi/\beta)] \quad \text{for} \quad X_3 < 0, \tag{A1}$$

where φ is the angle between the X_1-axis and the propagation direction of the incident plane wave. Because $\partial/\partial X_2 = 0$ for a 2-D elastic medium, the equations of motion are

$$\left(\rho \frac{\partial^2}{\partial t^2} - c_{2k2n} \frac{\partial^2}{\partial X_k \partial X_n}\right) u_2 = 0, \quad k, n = 1, 3, \tag{A2}$$

where ρ is the density, c_{2k2n} are the elastic constants, u_2 is the X_2 component of the displacement and the summation convention is understood. The solutions of eq. (A2) can be written as

$$u_2(X_1, X_3) = a_2 \exp[-i\omega(t - q_k X_k)], \tag{A3}$$

where a_2 is the amplitude, and q_1 and q_3 are the slowness in the X_1 and X_3 directions, respectively. By substituting eq. (A3) into eq. (A2), we obtain

$$(\rho - c_{2k2n} q_k q_n) a_2 = 0. \tag{A4}$$

For non-zero a_2 we require

$$\rho - c_{1212} q_1^2 - 2c_{1223} q_1 q_3 - c_{2323} q_3^2 = 0. \tag{A5}$$

Thus three elastic constants, c_{1212}, c_{1223} and c_{2323} are necessary for a *SH* plane wave propagation in a 2-D anisotropic medium. Since the slowness in the X_1 direction is given by

$$q_1 = \cos\varphi/\beta, \tag{A6}$$

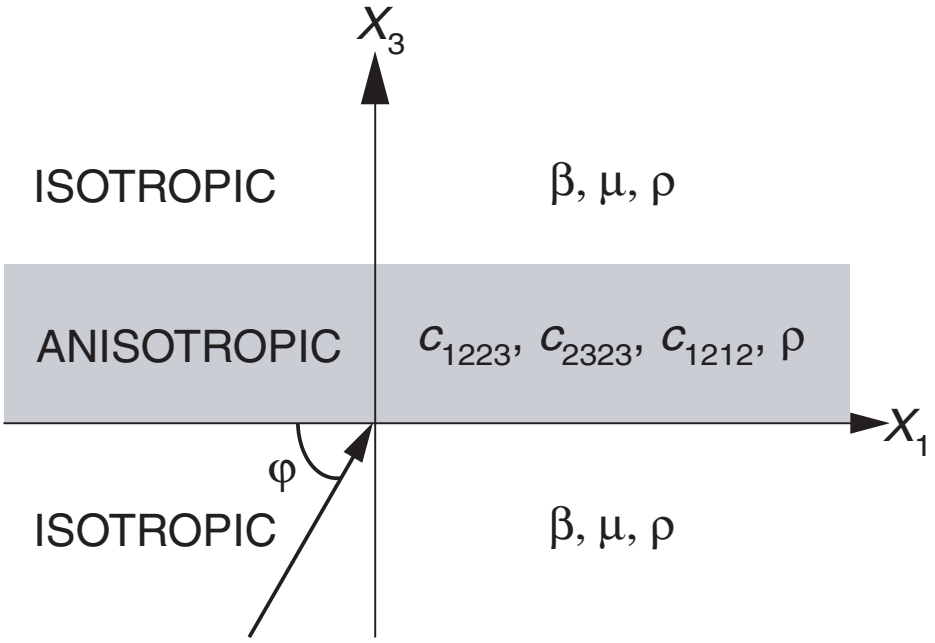

Figure A1. Definition of the coordinate system for an anisotropic medium equivalent to the cracked zone shown in Fig. 1.

eq. (A5) is a quadratic equation for q_3 with real coefficients. Now we assume an anisotropic medium, where a *SH* plane wave propagates in the X_1 direction with the velocity β. For $\varphi = 0$, eq. (A5) is reduced to

$$\beta^2 c_{2323} q_3^2 + 2\beta c_{1223} q_3 + c_{1212} - \mu = 0, \tag{A7}$$

by substituting $q_1 = 1/\beta$ and using $\rho\beta^2 = \mu$, where μ is the rigidity. The two roots of eq. (A7) are obtained as

$$q_3 = \frac{-c_{1223} \pm \sqrt{c_{1223}^2 + c_{2323}(\mu - c_{1212})}}{\beta c_{2323}}, \tag{A8}$$

where $c_{2323} \neq 0$. Because both of them equal to 0 for $\varphi = 0$, we obtain

$$c_{1212} = \mu, \tag{A9}$$

$$c_{1223} = 0. \tag{A10}$$

Thus only the elastic constant c_{2323} is necessary to define the assumed anisotropic medium. By using eqs (A6), (A9) and (A10) the two roots of eq. (A5) are obtained as

$$q_3 = \pm \frac{\sin\varphi}{\beta} \sqrt{\frac{\mu}{c_{2323}}}. \tag{A11}$$

When the two roots represented by eq. (A11) are written as $q(1)$ and $q(2)$, which correspond to the propagation directions of $+X_3$ and $-X_3$, respectively, a general solution of eq. (A2) are written in the form

$$u_2(X_1, X_3) = \sum_{n=1}^{2} f(n) \exp[-i\omega(t - q_1 X_1 - q(n) X_3)], \tag{A12}$$

where $f(n)$ are relative excitation factors.

Next, we define a stress tensor τ_{jk}. Since we consider *SH* waves propagating in 2-D media, only one component is needed and given by

$$\tau_{32} = \tau_{23} = c_{1223} \frac{\partial u_2}{\partial X_1} + c_{2323} \frac{\partial u_2}{\partial X_3}. \tag{A13}$$

After using eq. (A12), eq. (A13) is reduced to

$$\tau_{23} = i\omega q_1 \sum_{n=1}^{2} f(n)(c_{1223} + c_{2323} q(n)/q_1) \times \exp[-i\omega(t - q_1 X_1 - q(n) X_3)]. \tag{A14}$$

We introduce the displacement-stress vector **w** and vector **f** of the excitation factors as follows:

$$\mathbf{w} = (u_2 \ \tau_{23}/i\omega q_1)^{\mathrm{T}}, \tag{A15}$$

$$\mathbf{f} = (f(1) \ f(2))^{\mathrm{T}}. \tag{A16}$$

The vector **f** in eqs (A12) and (A14) is related to the vector **w** at the interface ($X_3 = 0$) by

$$\mathbf{w} = \mathbf{E}\mathbf{f} \exp[-i\omega(t - q_1 X_1)], \tag{A17}$$

where the 2×2 matrix **E** is

$$\mathbf{E} = \begin{pmatrix} 1 & 1 \\ c_{1223} + c_{2323} q(1)/q_1 & c_{1223} + c_{2323} q(2)/q_1 \end{pmatrix}. \tag{A18}$$

In an isotropic medium, eq. (A5) becomes

$$\rho - \mu q_1^2 - \mu q_3^2 = 0 \tag{A19}$$

because of $c_{1212} = c_{2323} = \mu$ and $c_{1223} = 0$. Since q_1 is given by eq. (A6), eq. (A19) has the solutions

$$\left.\begin{aligned} q(1) &= \sin\varphi/\beta, \\ q(2) &= -\sin\varphi/\beta. \end{aligned}\right\} \tag{A20}$$

For an isotropic medium, the matrix **E** given in eq. (A18) becomes

$$\mathbf{E} = \begin{pmatrix} 1 & 1 \\ \mu\tan\varphi & -\mu\tan\varphi \end{pmatrix}. \tag{A21}$$

Now we refer to the lower and upper media as media 1 and 2, respectively. The displacement and stress are continuous across the

interface ($X_3 = 0$), so that the boundary condition is

$$\mathbf{E_1 f_1} = \mathbf{E_2 f_2}, \tag{A22}$$

where $\mathbf{E_j}$ and $\mathbf{f_j}$ are the matrix $\mathbf{E}$ and the vector of the excitation factors for the medium j ($j = 1, 2$), respectively.

The reflection and transmission coefficients are obtained by eq. (A22). When a *SH* plane wave is incident from an isotropic medium to an anisotropic medium, eq. (A22) can be written as

$$\begin{pmatrix} 1 & 1 \\ c_{1223} + c_{2323}q(1)/q_1 & c_{1223} + c_{2323}q(2)/q_1 \end{pmatrix} \begin{pmatrix} T \\ 0 \end{pmatrix} = \begin{pmatrix} 1 & 1 \\ \mu \tan\varphi & -\mu \tan\varphi \end{pmatrix} \begin{pmatrix} 1 \\ R \end{pmatrix}, \tag{A23}$$

where R and T are reflection and transmission coefficients at the interface. In the case of the plane wave incidence from an anisotropic medium to an isotropic medium, eq. (A22) becomes

$$\begin{pmatrix} 1 & 1 \\ c_{1223} + c_{2323}q(1)/q_1 & c_{1223} + c_{2323}q(2)/q_1 \end{pmatrix} \begin{pmatrix} 1 \\ R \end{pmatrix} = \begin{pmatrix} 1 & 1 \\ \mu \tan\varphi & -\mu \tan\varphi \end{pmatrix} \begin{pmatrix} T \\ 0 \end{pmatrix}. \tag{A24}$$

Once eqs (A23) and (A24) are solved, the reflection and transmission coefficients of an anisotropic layer can be obtained from those of the upper and lower boundaries of the anisotropic layer by the reflection and transmission operator method (Kennett 1984).

The *SH* wave velocity v_a in the anisotropic medium can be calculated from

$$1/{v_a}^2 = {q_1}^2 + {q_3}^2, \tag{A25}$$

where q_1 and q_3 are given by eqs (A6) and (A11) for an assumed φ. Eq. (A25) is reduced to

$$\frac{v_a}{\beta} = \frac{1}{\sqrt{\cos^2\varphi + \mu \sin^2\varphi / c_{2323}}}. \tag{A26}$$